JCTC Journal of Chemical Theory and Computation

LETTER

pubs.acs.org/JCTC

Bridging the Gap between Folding Simulations and Experiments: The Case of the Villin Headpiece

G. Saladino, M. Marenchino, and F. L. Gervasio*

Structural Biology and Biocomputing Programme, Spanish National Cancer Research Centre (CNIO), c/Melchor Fernandez Almagro 3, 28029, Madrid, Spain

Supporting Information

ABSTRACT: The increasing accuracy of molecular dynamics force fields parameters and the increasing resolution of experimental results allow one to carefully compare and complement in silico data with experimental observations. Here, we study the human villin headpiece C-terminal helical subdomain (HP35) with the recent highly optimized Amber99SB*-ILDN force field and compare the results with recent high resolution triplet−triplet energy transfer (TTET) experiments. The correct reproduction of the main structural features reveals a good agreement between experimental data and simulations.

1. INTRODUCTION

Understanding the mechanism of protein folding with high spatial and temporal resolution remains one of the most important and challenging goals of molecular biophysics and biophysical chemistry.[1] Thanks to the impressive progress in experimental techniques, such as as triplet−triplet energy transfer (TTET),[2] we now have access to very detailed information about the folding mechanisms. However, the atomistic interpretation of the spectroscopic observations can be complex and often requires the help of molecular modeling and simulations. Molecular dynamics (MD) simulations have been successfully used for studying complex biomolecular systems, providing an atomistic description of their structure and dynamics. Unfortunately, their predictive power has been so far hampered by the limited time-scale that they can routinely reach and by the accuracy of the force fields used. Recently, the development of advanced sampling algorithms,[3−5] the use of specialized hardware,[6] and the concomitant improvement of force fields[7−9] have extended the capability of MD simulations to the point that they can be directly used for interpreting and complementing the experiments. At the same time, a careful comparison of the simulation prediction with much more detailed experiments can be used to verify the quality of the latest force field.

Here, we take advantage of state-of-the-art simulation techniques to reinvestigate the mechanism of folding of the human villin headpiece C-terminal helical subdomain (HP35)[10] in water and compare it with high resolution spectroscopy experiments[2] and CD measurements. Our converged free energy surfaces agree surprisingly well with the experiments, showing a rather dynamic folded state and an unfolded ensemble that retains significant structure.

2. RESULTS

2.1. Different Conformations of HP35. HP35 has a well-defined secondary and tertiary structure, characterized by three α helices bundled together by a closely packed hydrophobic core involving three phenylalanines,[11] and is one of the smallest peptides that folds cooperatively.[12] Because of its small size and fast folding dynamics, HP35 has been the subject of several computational[13−19] and experimental[2,11,20−27] studies. We performed 1.5-μs-long unbiased fully atomistic MD simulations, massive bias exchange molecular dynamics simulations (BEMD)[28] at 298 and 320 K, and calorimetry and circular dichroism (CD) experiments. Fully atomistic MD simulations were performed at 298 K starting from the lowest energy NMR structure (PDB code: 1UNC).[10] We used the most recent Amber99SB*-ILDN[29] force field, including improved rotamer[7] and backbone corrections.[8]

During the simulation, we observed only partial unfolding and refolding events. The simulation spends most of the time in two folded structures that differ in the "compactness" of the hydrophobic core, while retaining all the secondary structure elements. This observation is in agreement with TTET experiments on HP35 folding, which have shown the presence of two folded states, N and N′, where the latter is less compact than the former.[2] Analysis of the conformations with the highest root mean square deviation (RMSD) from the NMR structure revealed the presence of a partially folded state, in which helixes 1 and 2 are correctly folded while helix 3 is largely unstructured. The higher stability of the region encompassing helixes 1 and 2 has been previously observed with both TTET and NMR.[2,23] It is worth noting that very long unbiased MD simulations at high temperature (380 K) performed with the same Amber99SB*-ILDN force field predicted that in the unfolded state the fraction of residues of helix 3 that are helical is larger than that of helix 1 and helix 2.[9]

To reconstruct a fully converged free-energy landscape of HP35 folding, we used massive BEMD simulations at 298 and 320 K, which is very close to the experimental melting temperature (see Supporting Information). Using BEMD, Piana et al.[19] were able to correctly predict the effects of a point mutation on HP35 in agreement with NMR and CD experiments. The BEMD runs were performed using the PLUMED[30] plug-in. The same

Received: April 12, 2011
Published: July 27, 2011

collective variables (CVs) of ref 19 were used. Each BEMD simulation required considerably longer sampling time than those used in ref 19 to converge (>300 ns). This is most probably due to the different version of the Amber force field used. Indeed, the folding time reported in ref 9 is 0.8 μs for Amber03 and 3.0 μs for Amber99*SB-ILDN. The free energy profiles were reconstructed from the unbiased probability distribution of the states of the neutral (unbiased) replica.

The existence of the two previously identified folded structures is confirmed by the free energy landscapes at 320 K. The representative structures of the two nearby free-energy basins correspond to the definition of the folded states N and N′ with the latter conformation, previously described as a "dry molten globule", being more open and more flexible (see Figure 1).[2] The solvent -accessible surface area (SASA) for the N′ conformation is 3109 Å^2, slightly more than the corresponding value (3056 Å^2) for the N state (Supporting Information, Figure S1). On average, the N′ state also shows an increase of the distance between the C- and N-termini compared to the N state (24.0 Å vs 18.7 Å), in agreement with experimental observations. As another point of agreement, half of the total SASA exposed during unfolding ($\Delta SASA_{N\rightarrow U}$ = 283 Å^2) is exposed during the N to N′ transition ($\Delta SASA_{N\rightarrow N'}^{max}$ = 123 Å^2).

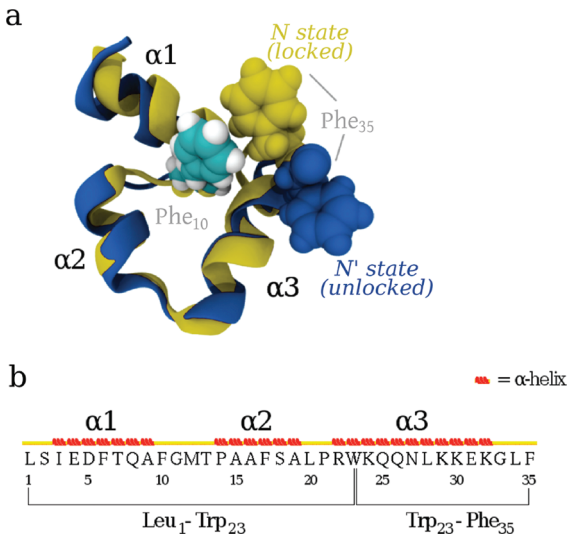

Figure 1. HP35 sequence and tridimensional structure. Two different folded states, N and N′, were observed. In agreement with ref 2, a locking mechanism exists involving the stacking of Phe_{10} and Phe_{35}.

For a punctual comparison with the high resolution experiment results, we calculated the free energy as a function of the set of distances measured in the TTET experiments and the C_α RMSD from the NMR structure. The distance between residues Trp_{23} and Phe_{35} was found to be the most suitable variable to discern the different conformations of HP35. The free energy at 320 K as a function of the Cα RMSD and the distance Trp_{23}—Phe_{35} is shown in Figure 2. Again two well-defined minima corresponding to the N and N′ states are observed: as opposed to the narrow N state minimum, the N′ state shows a wider free energy basin, confirming its increased flexibility. As suggested by Kiefhaber et al., the N and N′ conformations are very similar, reporting an overall Cα RMSD of 0.9 Å.

The calculation of relevant residues' distances and RMSDs for both conformations reveals that the structural differences between N and N′ are due to the stacking of the aromatic rings of Phe_{10} and Phe_{35}, responsible for the observed slightly more compact structure in which the orientation of helix 1 slightly changes (Figure 1).

Besides the clearly visible N and N′ states, a secondary partially folded minimum can be observed. This minimum, corresponding to a Trp_{23}—Phe_{35} distance of 9.85 Å, versus 15.22 Å of the native state, is populated by conformations in which helix 3 is partially unfolded (Supporting Information Figure S2). Its conformation strongly resembles the intermediate state I proposed in ref 2 and is consistent with the intermediate state proposed by Eaton et al.[26] and with the observed relative stability of the three helices.[23,25]

This confirms the observation done in the unbiased MD run at 298 K and is at odds with the results of unbiased MD runs at 380 K. The difference in relative helix stability could be due to the temperature. However, as we perform a biased MD simulation, we are only able to reconstruct the thermodynamics of the system, not the kinetics. Thus, we can only hypothesize that the I state that we observe is an off-path intermediate.

The free energy profile as a function of RMSD and the distance between residues Leu_1 and Trp_{23} shows once more two minima corresponding to the folded ensemble (low RMSD values and NMR Leu_1—Trp_{23} distance) together with a broad minimum corresponding to an unfolded structure (high RMSD and low Leu_1—Trp_{23} distance).

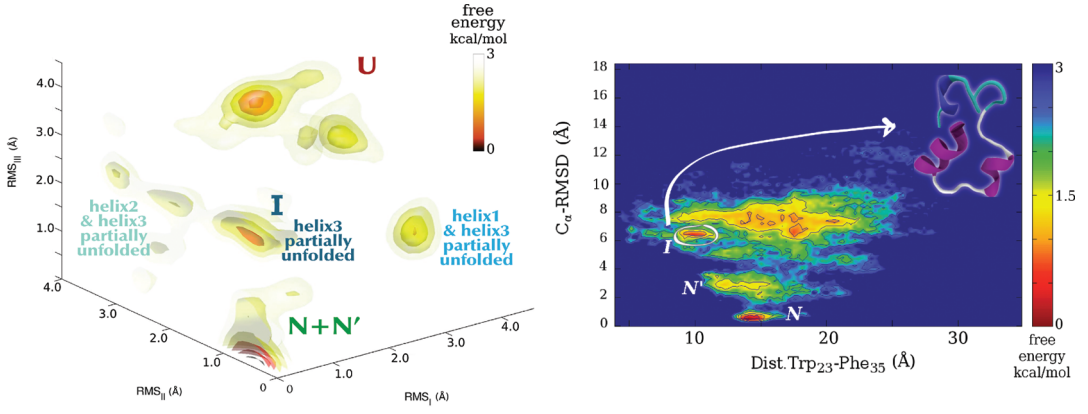

Figure 2. Left: HP35 free energy landscape at 320 K as a function of the RMSD from the ideal helical structure of the three helices. Right: Free energy landscape at 320 K projected on the distance between residues Trp_{23}-Phe_{35} and the RMSD of the Cα from the NMR native structure.

dx.doi.org/10.1021/ct2002489 |J. Chem. Theory Comput. 2011, 7, 2675–2680

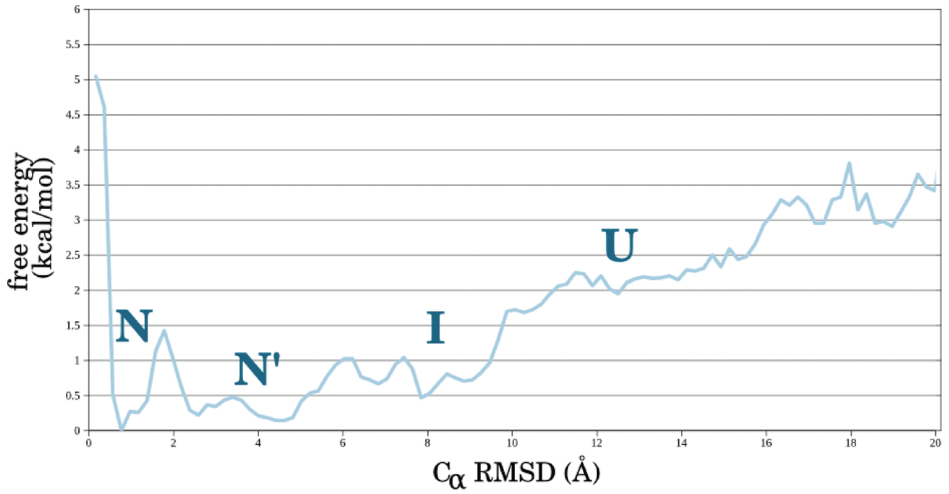

Figure 3. Free energy profile at 298 K as a function of the Cα RMSD. The relative stability of conformations N, N′, I, and U is very similar to that found in the experiments (see ref 2).

The structures found in the unfolded basin are consistent with the well-documented observations of residual helical structure in the unfolded ensemble of HP35.[23,25,31−33] The free energy as a function of the helical content (see Supporting Information Figure S3) shows two minima corresponding respectively to the value typical of the folded structure and to a higher helical content. The absence of a minimum corresponding to low helical content means that random coil structures are much higher in energy. This confirms the propensity of HP35 to adopt partially structured conformations in the unfolded ensemble instead of a random coil.

Overall, the conformations observed in TTET experiments are correctly identified in our simulations. However, at 320 K, the relative stability of the various conformations does not agree with that of the experiments, where the N and N′ states have almost the same stability, while the I state is scarcely populated (see Figure 2). Moreover, the stability order of the helices at 320 K does not correspond to that predicted at 380 K with very long unbiased MD simulations.

To assess whether these discrepancies are due to the different temperature of the simulations and the TTET experiments or to the force field, we repeated the BEMD simulation at 298 K. At this temperature, the main features of the FES, as well as the conformations of the N and N′ states, are conserved. On the contrary, the relative stability is now in better agreement with the experiments (as expected). The relative stability at 298 K is N < N′ ≪ I (see Figure 3).

While the agreement with experiments is recovered, not all is well with respect to the population of the I state as a function of the temperature. Indeed, TTET experiments suggest that, at higher temperatures, the population of the N′ state increases, while the I state remains scarcely populated, and the BEMD simulations predict that the population of the I state at 320 K is still significant, to the detriment of the N′ state.

We found that the calculated activation energies are lower that the experimental values. Nevertheless, the order observed in the experiments is reproduced, confirming that the N→N′ barrier is high (5.9 kJ/mol) and higher than the N′→I one (3.78 kJ/mol). Thus, the unfolding of helix α_3 is fast once the system reaches the unlocked N′ state and much faster than the N→N′ rearrangements, as observed experimentally. Our results suggest that the unfolding of HP35 should involve a three-step mechanism: unlocking (→N′), unfolding of helix α_3 (→I), and overall unfolding (→U). However, as mentioned, it is difficult to discern from BEMD simulations whether the unfolding of helix α_3 is part of the overall unfolding process or a competitive process leading to an off-path intermediate. Considering the kinetics of the process, these results are in agreement with ref 2, suggesting that the N→N′ conformational change can constitute a rate limiting step in fast-folder variants of HP35.

2.2. The Locking Mechanism for Native states N and N′. We carefully analyzed the differences between the states N and N′ performing two additional 100 ns unbiased MD simulations. No transitions were observed in either MD, confirming that the two structures are stable states and in agreement with the experimentally measured interconversion characteristic time of 900 ns (see ref 2). The unbiased MDs allowed for a better characterization of the differences between N and N′. As observed in the BEMD simulations, the stacking of Phe_{35} onto Phe_{10} is the most evident difference. However, the equilibrium MD revealed that Phe_{35} stacking is a faster movement compared to the N→N′ transition, as detachment and restacking of Phe_{35} was observed multiple times during the 100 ns. Hence, Phe_{35}−Phe_{10} interaction, while being a well-defined feature of the N state, seems to be involved in the locking mechanism but not univocally identifiable with it. In a previous work, Pande et al.[14] suggested that the stacking of Phe_{10} and Phe_{35} constitutes a kinetic trap since their strong interaction prevents HP35 from adopting a correct folding. However, it was proven experimentally[21] that mutation of residue Phe_{35} does not cause considerable alteration of folding kinetics. The fast kinetics of Phe_{35} observed in our simulations thus put into perspective the results previously obtained: while important and characteristic of the N state, the Phe_{35}−Phe_{10} interaction is fast enough not to be determinant for folding kinetics.

A deeper analysis of the interactions in the "lock region", where the terminal residues of helix α_1 are in contact with the C-terminal region belonging to helix α_3, comprising residues 8−11 and 32−35, respectively, revealed the presence of a complex network of hydrogen bonds. A highly populated (>42 %) H bond between Ala_9 and Leu_{34} was observed. This H bond is almost as strong as the *i*, *i* + 4 α-helical bonds, keeping

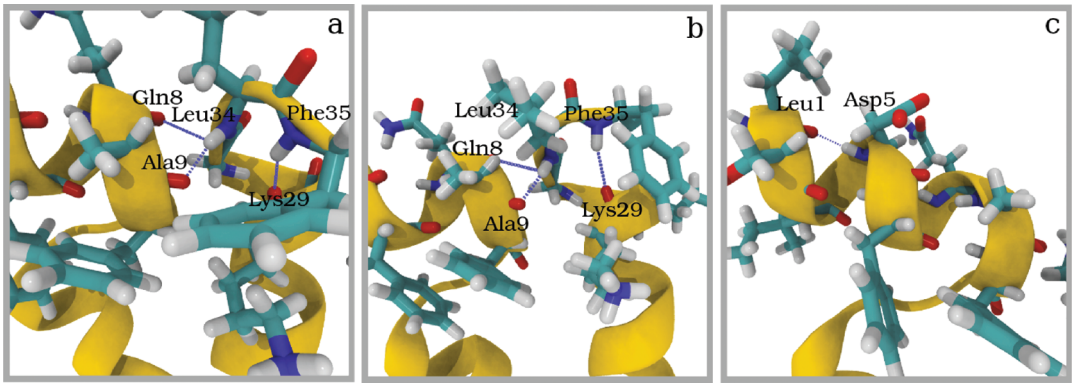

Figure 4. The residues involved in the locking mechanism. (a) H-bond network involving residues Gln_8, Ala_9, and Leu_{34}. (b) The strong H bonds are preserved even when Phe_{35} briefly detaches from the hydrophobic core. (c) As opposed to the N′ state, a strong *i*, *i* + 4 H bond is observed between residues Leu_1 and Asp_5 in the N state.

helices α_1 and α_3 close. Another strong H bond was observed between Gln_8 and Leu_{34}, with a population of 23.1 %. At least in 15% of the entire trajectory, Leu_{34} is involved in a bifurcated H bond involving both residues (see Figure 4, panel a).

A strong H bond was also observed between Phe_{35} and Lys_{29} (Figure 4, panel a); this *i*, *i* + 6 bond forces a particular conformation of the C terminus, where the backbone forms an additional "helix-like" turn. The identified H-bond network was never completely broken throughout our 100 ns simulation of the N state, even when Phe_{35} breifly undocks (see Figure 4, panel b), thus proving to be the slow-kinetic step involved in the "locking" mechanism. This is confirmed by the analysis of the N′ state conformations. In this case, none of the mentioned H bonds has a population higher then 1.8%, helices α_1 and α_3 are detached, and the C-terminal region is extremely more flexible, as observed in TTET experiments (see ref 2 and Supporting Information Figure S4).

The stacking of Phe_{35} onto Phe_{10} is not observed anymore, and Leu_{34} substitutes Phe_{35} in the strong HP35 hydrophobic core (see Supporting Information Figure S5). In the 75% of the conformations, Phe_{35} does not point toward the hydrophobic core, as in the N state, but toward the back side of helix α_1. Surprisingly, in this conformation Phe_{35} forms strong H-bonds with the residues left unpaired by Leu_{34}, Gln_8 (pop. 32.47%), and Ala_9 (pop. 7.99%; see Supporting Information Figure S6). Interestingly, the interaction of Phe_{35} with the side of helix α_3 destabilizes the first turn of helix α_1, as the population of the first *i*, *i* + 4 α-helical bond between Leu_1 and Asp_5 drops from the 57% of the N state to 31.8%. This gives rise to a quite different conformation of state N′ in the N-terminal region as well (see Supporting Information Figure S7).

Analyses of the N′ conformations also prompted an additional striking point toward the agreement with the experiments: conformations with a very low distance between residues Trp_{23} and Phe_{35} were observed, in which the C-terminal region unwinds on top of helix α_3 (see Supporting Information Figure S8). These conformations explain why TTET experiments observed more rapid exchanges between Nal23−Xan35 in the N′ state.

3. EXPERIMENTAL VALIDATION

So far, the simulations provided a very detailed view of the molecular structure and dynamics that at room temperature is in excellent agreement with spectroscopic observations. Still, as the temperature increases, the behavior seems to depart from that experimentally observed. To further investigate this issue, we performed thermodynamic and spectroscopic measurements. HP35 in water has a well-defined structure, as shown by the CD spectra with two minima at 208 and 222 nm and a positive band near 190 nm, characteristic of the α-helical structure (Figure 5). The ratio of those minima, $\theta_{222:208}$ has been used as a criterion in several proteins to evaluate the presence of coiled-coil helices. For a noninteracting α helix, the ratio has been shown to be 0.83, while for stranded coiled coils, the ratio was calculated to be >1.[34−38] HP35 in water exhibited a $\theta_{222:208}$ ratio above 1 up to 50 °C. Then, we exploited thermal and chemical denaturation to gain an in-depth thermodynamic description. Under all conditions tested, HP35 showed a cooperative, sigmoidal transition, and the data fit a two-state model with a transition temperature (T_m) of 44 °C. Chemical denaturation experiments using urea were also carried out at seven different temperatures ranging from 10 to 40 °C. The addition of urea resulted in the loss of secondary structure, and the denaturation curve, as determined by following the dichroic signal at 222 nm, also showed two-state unfolding behavior. At 25 °C, the midpoint of the urea-induced unfolding transition

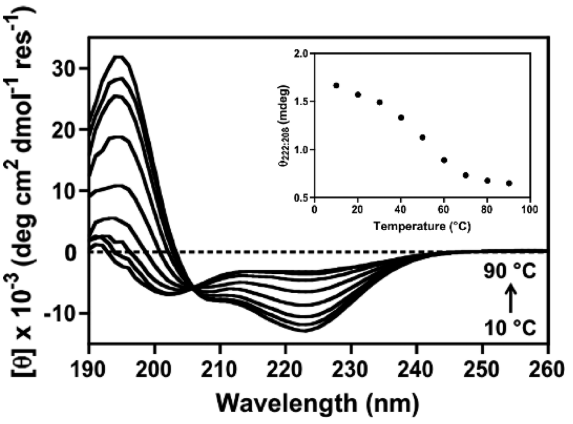

Figure 5. Far-UV CD spectra and $\theta_{222:208}$ ratio of HP35 in water as a function of temperature. Superimposition of the spectra acquired at different temperatures reveals the presence of an isodichroic point at 206 nm, indicative of a two-state unfolding of the protein.

Table 1. Thermodynamic Parameters for HP35 in Pure Water[a]

ΔH	ΔC_p	T_m (°C)	$\Delta G_{47°C}{}^{b}$	$\Delta G^{calc}_{47°C}{}^{c}$
24.8 ± 0.9	0.37 ± 0.06	44 ± 0.1	−0.24	−0.04

[a] Energies are in kcal mol^{-1}, C_p in kcal mol^{-1} K^{-1}, and temperature in °C. [b] Obtained from the experiments employing the Gibbs−Helmholtz equation. [c] Obtained by integration of the folded and unfolded basins in a tridimensional free energy projected as a function of the RMSD from a perfect α helix for the three helical segments of HP35.

is 2.9 M. From the combination of the change in Gibbs free energy upon thermal and chemical denaturation, we obtained the stability plot of HP35 (Supporting Information Figure S5), calculated the change of the unfolding free energy at 320 K, and compared it to the calculated value (Table 1). The agreement is surprisingly good, given reports of an overestimation of melting temperatures by various force fields.[6,8,39−45]

In conclusion, state-of-the-art simulations and recently improved force fields not only are able to reproduce the main structural features of HP35 folding in water but also to quantitatively predict the folding free energy landscape. Our simulations were able to interpret the postulated locking mechanism interconverting the two folded structures (open and closed), which involves the breaking of a strong hydrogen bond network involving residues Gln_8, Ala_9, and Leu_{34} and the stacking of Phe_{10} and Phe_{35} residues. Thermodynamics data obtained by CD were also found to be in surprisingly good agreement with the corresponding calculated values, showing that the latest correction to the Amber99SB*-ILDN force field does improve its predictive power in folding simulations. However, the relative stability of the three helices seems to be dependent on the temperature,[9] an issue that is worth analyzing in future studies.

■ ASSOCIATED CONTENT

Supporting Information. Computational and experimental methods, an experimental stability curve obtained through thermal and chemical denaturation, together with additional figures describing the main differences between the different conformations of HP35. This information is available free of charge via the Internet at http://pubs.acs.org/.

■ AUTHOR INFORMATION

Corresponding Author

*E-mail: flgervasio@cnio.es.

■ ACKNOWLEDGMENT

We acknowledge support by the Spanish Science and Innovation (MICINN) grant (BIO2010-20166, "AlteredDynamics"). G.S. acknowledges the European Commission Capacities Area - Research Infrastructures Initiative HPC-EUROPA2 (project number: 228398) for partial support. The Barcelona Supercomputing Center is acknowledged for a generous allocation of computer resources.

■ REFERENCES

(1) Shakhnovich, E. *Chem. Rev.* **2006**, *106*, 1559–88.
(2) Reiner, A.; Henklein, P.; Kiefhaber, T. *Proc. Natl. Acad. Sci. U.S.A.* **2010**, *107*, 4955–4960.
(3) Laio, A.; Gervasio, F. L. *Rep. Prog. Phys.* **2008**, *71*, 126601.
(4) Bonomi, M.; Branduardi, D.; Gervasio, F. L.; Parrinello, M. *J. Am. Chem. Soc.* **2008**, *130*, 13938–13944.
(5) Saladino, G.; Pieraccini, S.; Rendine, S.; Recca, T.; Francescato, P.; Speranza, G.; Sironi, M. *J. Am. Chem. Soc.* **2011**, *133*, 2897–2903.
(6) Shaw, D. E.; Maragakis, P.; Lindorff-Larsen, K.; Piana, S.; Dror, R. O.; Eastwood, M. P.; Bank, J. A.; Jumper, J. M.; Salmon, J. K.; Shan, Y.; Wriggers, W. *Science* **2010**, *330*, 341–346.
(7) Lindorff-Larsen, K.; Piana, S.; Palmo, K.; Maragakis, P.; Klepeis, J. L.; Dror, R. O.; Shaw, D. E. *Proteins: Struct. Funct. Bioinf.* **2010**, *78*, 1950–8.
(8) Best, R. B.; Buchete, N. V.; Hummer, G. *Biophys. J.* **2008**, *95*, L07–L09.
(9) Piana, S.; Lindorff-Larsen, K.; Shaw, D. E. *Biophys. J.* **2011**, *100*, L47–9.
(10) Vermeulen, W.; Vanhaesebrouck, P.; Troys, M. V.; Verschueren, M.; Fant, F.; Goethals, M.; Ampe, C.; Martins, J. C.; Borremans, F. A. M. *Protein Sci.* **2004**, *13*, 1276–1287.
(11) Chiu, T. K.; Kubelka, J.; Herbst-Irmer, R.; Eaton, W. A.; Hofrichter, J.; Davies, D. R. *Proc. Natl. Acad. Sci. U.S.A.* **2005**, *102*, 7517–22.
(12) McKnight, C. J.; Doering, D. S.; Matsudaira, P. T.; Kim, P. S. *J. Mol. Biol.* **1996**, *260*, 126–34.
(13) Duan, Y.; Kollman, P. A. *Science* **1998**, *282*, 740.
(14) Zagrovic, B.; Snow, C. D.; Shirts, M. R.; Pande, V. S. *J. Mol. Biol.* **2002**, *323*, 927–937.
(15) Ripoll, D.; Vila, J.; Scheraga, H. *J. Mol. Biol.* **2004**, *339*, 915–925.
(16) Mori, G. M. D.; Micheletti, C.; Colombo, G. *J. Phys. Chem. B* **2004**, *108*, 12267–12270.
(17) Lei, H.; Wu, C.; Liu, H.; Duan, Y. *Proc. Natl. Acad. Sci. U.S.A.* **2007**, *104*, 4925.
(18) Yang, J. S.; Wallin, S.; Shakhnovich, E. I. *Proc. Natl. Acad. Sci. U.S.A.* **2008**, *105*, 895–900.
(19) Piana, S.; Laio, A.; Marinelli, F.; Troys, M. V.; Bourry, D.; Ampe, C. *J. Mol. Biol.* **2008**, 460–470.
(20) Frank, B. S.; Vardar, D.; Buckley, D. A.; McKnight, C. J. *Protein Sci.* **2002**, *11*, 680–7.
(21) Kubelka, J.; Eaton, W. A.; Hofrichter, J. *J. Mol. Biol.* **2003**, *329*, 625–30.
(22) Wang, M.; Tang, Y.; Sato, S.; Vugmeyster, L.; McKnight, C.; Raleigh, D. *J. Am. Chem. Soc.* **2003**, *125*, 6032–6033.
(23) Tang, Y.; Rigotti, D.; Fairman, R.; Raleigh, D. *Biochemistry* **2004**, *43*, 3264–3272.
(24) Brewer, S. H.; Vu, D. M.; Tang, Y.; Li, Y.; Franzen, S.; Raleigh, D. P.; Dyer, R. B. *Proc. Natl. Acad. Sci. U.S.A.* **2005**, *102*, 16662–7.
(25) Havlin, R. H.; Tycko, R. *Proc. Natl. Acad. Sci. U.S.A.* **2005**, *102*, 3284–9.
(26) Kubelka, J.; Henry, E. R.; Cellmer, T.; Hofrichter, J.; Eaton, W. A. *Proc. Natl. Acad. Sci. U.S.A.* **2008**, *105*, 18655–62.
(27) Bunagan, M.; Gao, J.; Kelly, J.; Gai, F. *J. Am. Chem. Soc.* **2009**, *131*, 7470–7476.
(28) Piana, S.; Laio, A. *J. Phys. Chem. B* **2007**, *111*, 4553–4559.
(29) Hornak, V.; Abel, R.; Okur, A.; Strockbine, B.; Roitberg, A.; Simmerling, C. *Proteins: Struct. Funct. Bioinf.* **2006**, *65*, 712–725.
(30) Bonomi, M.; Branduardi, D.; Bussi, G.; Camilloni, C.; Provasi, D.; Raiteri, P.; Donadio, D.; Marinelli, F.; Pietrucci, F.; Broglia, R. A.; et al. *Comput. Phys. Commun.* **2009**, *180*, 1961–1972.
(31) Tang, Y.; Goger, M. J.; Raleigh, D. P. *Biochemistry* **2006**, *45*, 6940–6.
(32) Wickstrom, L.; Okur, A.; Song, K.; Hornak, V.; Raleigh, D. P.; Simmerling, C. L. *J. Mol. Biol.* **2006**, *360*, 1094–1107.
(33) Rajan, A.; Freddolino, P. L.; Schulten, K. *PLoS ONE* **2010**, *5*, e9890.
(34) Zhou, N.; Kay, C.; Hodges, R. *J. Biol. Chem.* **1992**, *267*, 2664–2670.
(35) Lau, S.; Taneja, A.; Hodges, R. *Biophys. J.* **1984**, *45*, A109–A109.
(36) Choy, N.; Raussens, V.; Narayanaswami, V. *J. Mol. Biol.* **2003**, *334*, 527–539.
(37) Thévenin, D.; Lazarova, T.; Roberts, M. F.; Robinson, C. R. *Protein Sci.* **2005**, *14*, 2177–2186.

(38) Marenchino, M.; Armbruster, D. W.; Hennig, M. *Protein Express. Purif.* **2009**, *63*, 112–119.
(39) Zhou, R. *Proc. Natl. Acad. Sci. U.S.A.* **2003**, *100*, 13280–5.
(40) Jas, G. S.; Kuczera, K. *Biophys. J.* **2004**, *87*, 3786–3798.
(41) Pitera, J. W.; Swope, W. *Proc. Natl. Acad. Sci. U.S.A.* **2003**, *100*, 7587–92.
(42) Nymeyer, H.; Garca, A. E. *Proc. Natl. Acad. Sci. U.S.A.* **2003**, *100*, 13934–9.
(43) Best, R. B.; Hummer, G. *J. Phys. Chem. B.* **2009**, *113*, 9004–15.
(44) Ghosh, T.; Garde, S.; Garca, A. E. *Biophys. J.* **2003**, *85*, 3187–93.
(45) Paschek, D.; Nymeyer, H.; Garca, A. E. *J. Struct. Biol.* **2007**, *157*, 524–33.